

# Characterization of a soft tissue-mimicking agar/wood powder material for MRgFUS applications

Theocharis Drakos<sup>a</sup>, Marinos Giannakou<sup>a</sup>, Georgios Menikou<sup>b</sup>, Georgios Constantinides<sup>c</sup>, Christakis Damianou<sup>d,\*</sup>

<sup>a</sup> MEDSONIC LTD, Limassol, Cyprus

<sup>b</sup> Medical Physics Sector, State Health Services Organization, Nicosia General Hospital, Nicosia, Cyprus

<sup>c</sup> Department of Mechanical Engineering and Materials Science and Engineering, Cyprus University of Technology, Limassol, Cyprus

<sup>d</sup> Department of Electrical Engineering, Computer Engineering and Informatics, Cyprus University of Technology, Limassol, Cyprus

## ARTICLE INFO

### Keywords:

Tissue-mimicking materials

Agar

Ultrasound

MRgFUS

## ABSTRACT

This study describes the development and characterization of an agar-based soft tissue-mimicking material (TMM) doped with wood powder destined for fabricating MRgFUS applications. The main objective of the following work was to investigate the suitability of wood powder as an inexpensive alternative in replacing other added materials that have been suggested in previous studies for controlling the ultrasonic properties of TMMs. The characterization procedure involved a series of experiments designed to estimate the acoustic (attenuation coefficient, absorption coefficient, propagation speed, and impedance), thermal (conductivity, diffusivity, specific heat capacity), and MR properties ( $T_1$  and  $T_2$  relaxation times) of the wood-powder doped material. The developed TMM (2% w/v agar and 4% w/v wood powder) as expected demonstrated compatibility with MRI scanner following images artifacts evaluation. The acoustic attenuation coefficient of the proposed material was measured over the frequency range of 1.1–3 MHz and found to be nearly proportional to frequency. The measured attenuation coefficient was 0.48 dB/cm at 1 MHz which was well within the range of soft tissue. Temperatures over 37 °C proved to increase marginally the attenuation coefficient. Following the transient thermoelectric method, the acoustic absorption coefficient was estimated at 0.34 dB/cm-MHz. The estimated propagation speed (1487 m/s) was within the range of soft tissue at room temperature, while it significantly increased with higher temperature. The material possessed an acoustic impedance of 1.58 MRayl which was found to be comparable to the corresponding value of muscle tissue. The thermal conductivity of the material was estimated at 0.51 W/m K. The measured relaxation times  $T_1$  (844 ms) and  $T_2$  (66 ms) were within the range of values found in the literature for soft tissue. The phantom was tested for its suitability for evaluating MRgFUS thermal protocols. High acoustic energy was applied, and temperature change was recorded using thermocouples and MR thermometry. MR thermal maps were acquired using single-shot Echo Planar Imaging (EPI) gradient echo sequence. The TMM matched adequately the acoustic and thermal properties of human tissues and through a series of experiments, it was proven that wood concentration enhances acoustic absorption. Experiments using MR thermometry demonstrated the usefulness of this phantom to evaluate ultrasonic thermal protocols by monitoring peak temperatures in real-time. Thermal lesions formed above a thermal dose were observed in high-resolution MR images and visually in dissections of the proposed TMM.

## 1. Introduction

The need for developing novel diagnostic and therapeutic applications that demonstrate improved safety, efficiency, and specificity towards the battle against serious diseases is a matter of ongoing research. Although phantoms were initially developed, characterized, and

calibrated for ultrasound (US) imaging applications in the 60 s, there is still an undeniable need for developing new phantoms to fill the gap of emerging medical applications. Throughout the years, several efforts have been made by researchers towards developing anthropomorphic phantoms for medical teaching and imaging applications. In the field of High-Intensity Focused Ultrasound (HIFU), a reusable TMM that

\* Corresponding author.

E-mail addresses: [gmenicou@mphs.moh.gov.cy](mailto:gmenicou@mphs.moh.gov.cy) (G. Menikou), [g.constantinides@cut.ac.cy](mailto:g.constantinides@cut.ac.cy) (G. Constantinides), [christakis.damianou@cut.ac.cy](mailto:christakis.damianou@cut.ac.cy) (C. Damianou).

<https://doi.org/10.1016/j.ultras.2021.106357>

Received 26 May 2020; Received in revised form 29 December 2020; Accepted 6 January 2021

Available online 30 January 2021

0041-624X/© 2021 The Author(s).

Published by Elsevier B.V. This is an open access article under the CC BY-NC-ND license

(<http://creativecommons.org/licenses/by-nc-nd/4.0/>).

possesses thermal, mechanical, MR, and acoustic properties close to that of soft tissue is of outermost importance.

There are limited commercial phantom options available such as those by ONDA (Onda Corporation, 1290 Hammerwood Ave, Sunnyvale, CA 94089, USA) which are useful for Magnetic Resonance-guided Focused Ultrasound (MRgFUS) systems. Ideally, TMMs should have approximately the same ranges of the speed of sound, attenuation, absorption, and scattering coefficients as soft tissue. These features should be controllable using appropriate additives and the variability of their properties should be small at standard operating conditions.

Different types of phantoms can be found in the literature for reproducing soft tissue using different TMMs. These types of phantoms can be uniform single-component phantoms and more complex ones that mimic the specific anatomy of human tissue [1]. TMMs for MRgFUS applications present different advantages and disadvantages concerning preparation complexity, cost, and acoustic properties.

Gelatin has been widely used as a material to mimic soft tissue for US and MR imaging [2]. Gelatin-based TMMs demonstrate thermal repeatability for low acoustic power, exhibit a nearly linear stress-strain curve, provide a wide range of stiffness that is easily controllable whereas its preparation procedure is simple [3]. However, gelatin-based materials continue to stiffen over time and have a low melting point (45 °C) making them unsuitable for applications such as HIFU [4]. The attenuation coefficient of gelatin-based TMMs can be controlled by varying the amount of gelatin [5]. Amongst their reported disadvantages is that they are not always homogeneous and are susceptible to microbial and bacterial invasion [6].

Another TMM that is useful for testing MRgFUS applications is polyacrylamide. Polyacrylamide gels can be transparent thus allowing visual observation of the coagulated zone by adding some heat-sensitive contents such as bovine serum albumin (BSA) and egg-white [7–9]. The acoustic attenuation can be adjusted by using materials such as evaporated milk, intralipid, and corn syrup [10]. However, the addition of high concentration of these materials might affect the transparency of polyacrylamide gels. The coagulation temperature of these gels is comparatively higher than that of biological tissues leading to an inaccurate simulation of tissue coagulation during thermal therapies [7]. A serious safety disadvantage of polyacrylamide-based gels is that their main constituent acrylamide monomer is a known neurotoxin which is classified as a carcinogen [9]. This type of gels also exhibits a limited shelf life from several hours when exposed to air to a few weeks when stored in an airtight container [11]. ONDA Corporation produces commercially available polyacrylamide-based phantoms for characterizing ultrasonic protocols. The position and lesion shape evolution in the gel can be observed since it permanently turns opaque when temperature surpasses a threshold of 70 °C [12]. Therefore, these phantoms are used to perform quality assurance tests on HIFU systems and treatment protocol evaluation. Although polyacrylamide TMMs have a low attenuation coefficient, the addition of glass beads can be used to increase their attenuation coefficient and match the corresponding value of the human liver [8].

N-isopropylacrylamide (NIPAM) gels exhibit higher transparency at room temperature than egg white doped TMMs [13]. A large opacity change can be achieved even with a small temperature change. The formation of thermal lesion is a reversible effect making this type of TMM reusable and ideal to model the therapeutic effects of HIFU. Sun et al. [13] investigated only the ability of the NIPAM-based gel to form thermal lesions and it has not been characterized for its acoustical, thermal, and MR properties.

In a recent study by Eranki et al. [14], an MR-imageable and HIFU-compatible tissue-mimicking thermochromic acrylamide-based material was presented. Silicon dioxide and BSA were added to enhance ultrasound attenuation and MRI signal changes since the coagulation of BSA causes changes in  $T_2$  relaxation time. A thermochromic ink that changes color based on temperature change after HIFU exposure was also used. The TMM can permanently change color upon heating, thus providing

information on ablation volume geometry, spatial targeting accuracy, and quantification of heating. The thermochromic acrylamide-based material is potentially useful for testing MRgFUS applications but its use is hindered by the rather complex and long fabrication procedure.

Poly (vinyl alcohol) (PVA) materials have been also used in MR applications [15] and to mimic breast tissue [16]. PVA is a widely used non-toxic industrial material. The main disadvantage of these materials (in form of pure gel for 1–2 freeze–thaw cycles) is their low acoustic attenuation coefficient which is far lower than the majority of human soft tissue's attenuation coefficient [15]. However, with the addition of additives (enamel paint) and the increase in the number of freeze–thaw cycles, the attenuation can be further increased. The attenuation of a pure PVA-gel with 1 freeze–thaw cycle is stated to be very low at 0.075 dB/cm-MHz and increases to 0.28 dB/cm-MHz when the gel is produced with 4 freeze–thaw cycles [15]. The procedure to manufacture a pure PVA-based TMM is very long and can last for many days depending on the number of freeze–thaw cycles.

Tofu is another material used to develop TMM phantoms. Although Tofu is cheap and it is readily available, it exhibits a lower nonlinearity parameter compared to soft tissue [17]. The acoustic properties of Tofu are not adjustable and vary according to the brand of raw material and extraction method. It has also been reported that Tofu-based TMMs are susceptible to microbial invasion and their shelf life is limited [17]. However, Tofu's absorption and speed characterization replicate adequately the corresponding of human soft tissue.

Agar is also used for the development of phantoms destined for ultrasound imaging and HIFU applications. Agar-based TMMs need to be refrigerated for extending their shelf life and reusability [18]. Agar possesses a higher melting point and superior fracture toughness compared to gelatin gels of similar density and during ultrasound imaging, its echogenicity is similar to human soft tissue [18]. Amongst the advantages of agar against other TMMs is their faster production procedure, and low acoustic scattering coefficient [18,19]. A main limitation of agar is that it tends to be more expensive than gelatin. Agar-based TMMs doped with homogenized whole milk and bovine milk have an attenuation coefficient in the range of 0.35–0.4 dB/cm-MHz while the addition of evaporated milk increases the value to 0.8 dB/cm-MHz [19]. The speed of sound of pure agar-based gel (with 2% w/v agar) was estimated at 1490 m/s. According to this study [19], more agar percentage results in a higher speed of sound (1512 m/s for 7.5% w/v agar). An agar-based breast-mimicking material with the addition of silicon dioxide and evaporated milk was proposed for evaluation of focused US systems on patients with breast cancer [20]. Lately, Menikou et al. [21] introduced an agar-based head phantom with an attenuation coefficient close to the corresponding human attenuation value for HIFU applications.

There is limited literature on the effects of thermal, acoustic, mechanical, and MR properties of wood powder. The propagation speed and attenuation coefficient of various kinds of wood have been previously measured [22–24]. It has been shown that absorption linearly increases with frequency up to 4 MHz while the propagation speed is dependent on the moisture content of wood [25]. The density of wood powder and water absorption of wood powder composited with bagasse was calculated and compared to other materials [26]. The density of wood powder was found to be 0.42 gr/cm<sup>3</sup> and the water absorption in composite wood powder and bagasse was found to be 13.5% [26]. In a study by Ababneh [27], it was found that wood blocks (*Rhizophora* spp) are low-cost, stable over time and possible human breast tissue replicating material for MRI purposes.  $T_1$  and  $T_2$  relaxation times of wood were found to match closely the ones of breast tissue.

The purpose of this study aims to describe the development of a novel agar-based TMM doped with wood powder and test its suitability as such by characterizing its acoustic, thermal, and MR properties. The idea of using wood powder is to increase the absorption coefficient in a controllable manner with thermal properties similar to soft tissue. The associated  $T_1$  and  $T_2$  relaxation times control the image contrast of the

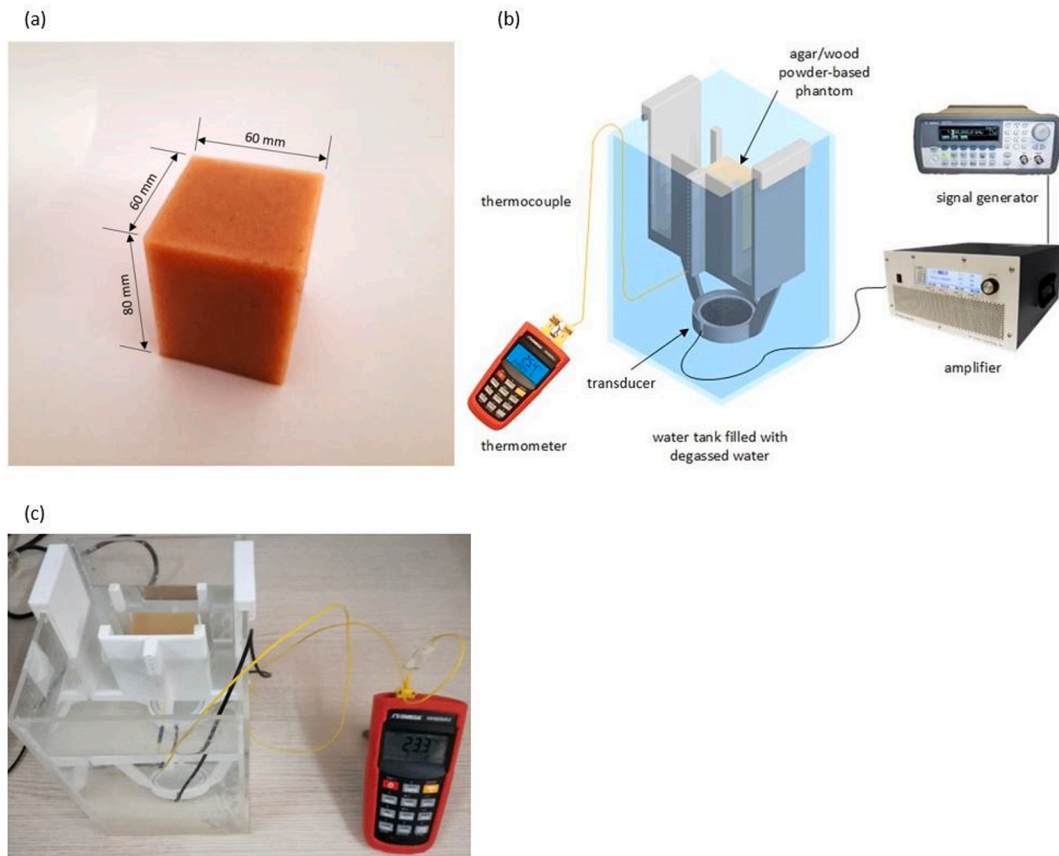


**Fig. 1.** (a) Photo of the developed agar/wood powder-based TMM, (b) schematic diagram of the experimental setup to measure the absorption coefficient of the TMM, and (c) photo of the experimental setup.

material in conventional MRI sequences. Wood powder is a very attractive additive since it is an abundant industrial furniture waste and most likely free of cost unlike other materials (silicon dioxide, BSA) which are more expensive and require difficult and long production procedures by the manufacturers.

Following test and trial, an appropriate agar concentration was selected to provide moderate strength to the final material in order to resist HIFU forces without cracking. The percentage of agar (2% w/v) was sufficient to create a compact material. It was chosen to avoid adding preservatives to the recipe to prolong the material's shelf-life since many of them are known of being toxic [28].

## 2. Materials and methods

### 2.1. Soft tissue-mimicking material preparation

The agar was in granular form with a particle size of 1400  $\mu\text{m}$  stated in the manufacturer's datasheet (Merck KGaA, EMD Millipore Corporation, Darmstadt, Germany). The agar was initially ground to powder using a blender machine to aid mixing in water and result in a homogeneous gel. Ultrapure degassed/deionized water was slowly heated and continuously stirred using a magnetic stirrer (SBS, A160, Steinberg Systems, Germany) over a period of 10 min. The temperature increase was monitored using an electronic thermometer (Omega Thermometer, HH806AU, Omega Engineering, Norwalk, Connecticut, USA). Once the degassed/deionized water reached 50  $^{\circ}\text{C}$ , 2% w/v agar was slowly added to mitigate aggregation of the agar in the degassed/deionized water. A certain amount of agar was added to the mixture to achieve a 2% w/v agar concentration. The wood powder (Swedish pine) was further ground with an average particle size of approximately 150  $\mu\text{m}$ . The average particle size was estimated by quantitative analyzing

images collected on a Scanning Electron Microscope (SEM) image (FEI, Quanta 200, Hillsboro, Oregon, United States), using the open-source software Gwyddion [29]. Prior to the SEM investigation, all samples were sputter-coated with a thin (<10 nm) silver layer to reduce electron charging effects. Images were collected at 5 kV to 20 kV accelerating voltages in various magnifications.

When agar was completely dissolved in water, a proportionate amount of wood powder (Swedish pine) was added to the mixture so that the w/v concentration of wood powder to be 4%. The mixture was stirred until the temperature reached 85  $^{\circ}\text{C}$ . The mixture began to solidify once the temperature dropped (at around 50  $^{\circ}\text{C}$ ). The amount of evaporated water added to equate the initial mixture volume prior to boiling initial volume. The solution was stirred with a low-speed setting to avoid trapping air bubbles in the mixture that would cause serious reflections of the HIFU beam. The whole preparation and development procedure was simple, fast, and it lasted around 20–25 min for a volume of 300  $\text{cm}^3$ . The solution was then poured into a mold ( $6 \times 6 \times 8 \text{ cm}^3$ ) and was let to jellify overnight at room temperature. The prepared phantom was tested in ablation experiments within 24 h after its fabrication.

The wood powder obtained from a carpentry company contained large pieces of particles that may have affected the acoustic properties of the developed TMM and induced susceptibility artifacts in MRI images. It was expected that since wood powder is poor in hydrogen it would appear hypointense in MRI images. The agar/wood powder TMM presented a moderate hardness along with a light brown color as shown in Fig. 1a.

### 2.2. Estimation of the attenuation coefficient

Attenuation measurements were conducted using the through-

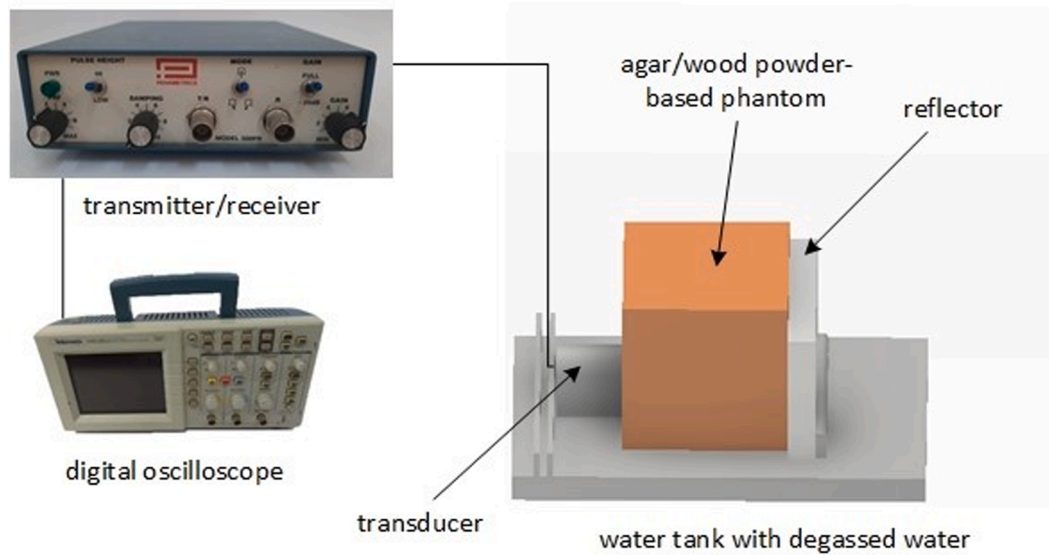


Fig. 2. Schematic diagram of the experimental setup to measure the ultrasonic propagation speed of the TMM.

transmission technique previously described by Madsen et al. [30]. The through-transmission technique involved two planar transducers; one for transmitting a pulsed US signal and one for receiving it. A special acrylonitrile butadiene styrene (ABS) plastic holder that hosts the two transducers, was designed (Inventor Professional 2018, Autodesk, California, USA) and printed using a 3D printer (F270, Stratasys Ltd., Minnesota, USA). The ABS holder retained the planar transducers in cylindrical cavities with their active elements facing each other and the sample at fixed positions. Three pairs of planar immersion transducers (12 mm diameter, nominal frequency at 1.1, 2 and 3 MHz, Piezotechnologies, Indianapolis, IN, USA) were used. All pairs of transducers have an approximate  $\pm 0.5$  MHz bandwidth, thus covering a 1–3 MHz span of frequencies. A pulsed signal was transmitted using a pulser/receiver system (Panametrics 500PR, Olympus Corp, Tokyo, Japan), propagated through a 26 mm sample and received by the receiving transducer which was located 65 mm from the transmitter. The attenuated resulting signal was recorded by the receiver and displayed on a digital oscilloscope (TDS 2012, Tektronix, Inc., Karl Braun Drive, United States). The sample was positioned in the near field of the emitting transducer. The attenuation coefficient was measured over a frequency range of 1.1–3 MHz at room temperature (25 °C) for five batches of gels. The following equation was used to calculate the attenuation coefficient for each frequency using the through-transmission method and it was modified into Eq. (1) in units of dB/cm [31].

$$\alpha(f) = \left( \frac{20 \cdot \log_{10} \left( \frac{A_s(f)}{A_r(f)} \right) \right)}{\Delta_x} \right) + \alpha_w \quad (1)$$

where  $A_s$  is the reference peak-to-peak voltage without the material,  $A_r$  is the resulting peak-to-peak voltage at the receiver side with the addition of the material between the two planar transducers,  $\alpha_w$  is the attenuation of water,  $\Delta_x$  is the sample's thickness in cm, and  $f$  is the transmitting frequency. The attenuation coefficient can be frequency-dependent according to  $\alpha = \alpha_0 \cdot f^n$ , where  $\alpha$  is the attenuation coefficient parameter,  $\alpha_0$  is the attenuation coefficient at 1 MHz, and  $n$  is the power to which frequency is raised in MHz. The impact of temperature on the attenuation coefficient was examined in a temperature range from 25 to 55 °C for the tested frequency of 1.1 MHz.

### 2.3. Estimation of the absorption coefficient

A method to estimate fast and accurately the absorption coefficient of the material using a novel experimental setup was previously described by our group [32]. According to this methodology, the material was exposed to a focused US beam and the absorption coefficient was determined by measuring the rate of temperature rise using a thermocouple (5SC-TT-K-30–36, type K insulated beaded wire, 100  $\mu$ m thick, Omega Engineering, Norwalk, Connecticut, USA). For the absorption coefficient measurement, a signal generator (HP 33120A, Agilent technologies, Englewood, CO, USA), an RF amplifier (AG1012, T & C Power Conversion, Inc., Humboldt St., Rochester, NY) and a spherically focused transducer (Sonic Concepts, Inc., Seattle, USA) operating at 0.4 MHz (focal length of 70 mm and diameter of 40 mm) were utilized in the experimental setup as described by Drakos et al. [32]. A temperature reader (HH806AU, Omega Engineering) was used to record the temperature over time in the TMM. The thermocouple was placed at the focal position which was located 3.5 cm deep from the bottom face of the TMM (the transducer was 3.5 cm below the front surface of the TMM facing upwards). Fig. 1 illustrates the schematic diagram (b) and a photo (c) of the experimental setup to estimate the absorption coefficient.

### 2.4. Estimation of acoustic propagation speed in soft tissue-mimicking material using the pulse-echo technique

A pulse-echo measurement immersion technique was employed for estimating the ultrasonic propagation speed of the TMM. The propagation speed was measured in a temperature range from 25 to 55 °C for the tested frequency of 1.1 MHz. The samples were immersed in a tank filled with degassed/deionized water. This technique involved a single unfocused transducer (the same transmitting transducer that was used for the attenuation measurements) to transmit and receive the reflected ultrasonic signal. The transducer transmitted pulses driven by a Panametrics pulser/receiver system (Panametrics 500PR, Olympus Corp). A digital oscilloscope (TDS 2012, Tektronix, Inc.) was connected to the pulser/receiver for observing the received signal. A thick sample of 5.8 cm was chosen to increase echoes time difference and derive a more accurate estimation of the ultrasonic propagation speed in the sample. As shown in Fig. 2, the signal was transmitted directly in the sample and reflected using a metal reflector. The propagation speed in the sample was estimated by measuring the time difference ( $\Delta_t$ ) between the echoes



returning from the interfaces of the sample. Eq. (2) was used to estimate the ultrasonic propagation speed ( $C_s$ ) of the TMM, where  $d$  represents the thickness of the sample.

$$C_s = \frac{2d}{\Delta_t} \quad (2)$$

### 2.5. Mass density measurement using water volume displacement method

Mass density was estimated by measuring the mass and volume of the samples. A 50 mL TMM was prepared and sliced in equal volumes to be placed inside a volumetric tube. Each piece was first weighed with a high precision ( $\pm 0.01$  g) digital scale (1479 V, Tanita Corporation of America, Inc, USA) and then its volume was extracted by measuring water displacement in a volumetric tube. The accuracy of the volumetric tube ( $\pm 0.1$  mL) played an important role in the error of the measurements, therefore large specimens were tested to minimize the fractional error in volume measurements. Five specimens from the same batch were obtained and the average mass density in  $\text{g/cm}^3$  was calculated.

### 2.6. Estimation of soft tissue-mimicking material thermal properties

The thermal properties of the aforementioned TMM were measured using the instrument Isomet (model 2104, Applied Precision, Ltd., Bratislava, Slovakia). The instrument was used according to the manufacturer's recommendation for estimating thermal conductivity (W/m K), thermal diffusivity ( $\text{mm}^2/\text{s}$ ), and specific heat capacity (kJ/kg K). The transient method was used to perform the thermal conductivity measurements, which were carried out automatically by a needle sensor. The selected sensor was able to accurately measure in the range of 0.2–1 W/m K. According to the manufacturer, the accuracy of the device for thermal conductivity measurements was 5% of reading  $+0.001$  W/m K. Thermal diffusivity is derived by dividing conductivity with density whereas specific heat capacity describes how quickly a material reacts to a change in temperature. A spherical volume of the material around the needle probe with a minimum diameter of 5 cm was needed for accurate measurement. Due to this limitation of the system, a specimen of appropriate dimensions (5 cm height, 7 cm wide, and 15 cm long) was prepared. The needle probe was inserted in the TMM and the 3 thermal properties (thermal conductivity, thermal diffusivity, and specific heat capacity) were calculated simultaneously by the device. The procedure was repeated five times and the mean and standard deviation values of each thermal property were deduced.

### 2.7. Experimental setup and HIFU sonication parameters

The absorption experimental setup described previously was used to apply high-power sonication in the phantom. The scope of the high-power sonication was to test the ability of the phantom to reach high temperatures and create lesions. The phantom was fitted tightly into the holder and a transducer (frequency 2.6 MHz, diameter: 38 mm, focal length: 61 mm, MEDSONIC LTD, Limassol, Cyprus) was positioned below the phantom facing upwards for a bottom to top sonication inside an acrylic water tank filled with degassed/deionized water. The experimental HIFU system included a signal generator (HP 33120A, Agilent Technologies), a radio-frequency power amplifier (AG1012, T & C Power Conversion, Inc.), and the spherically-focused transducer.

Prior to sonication, the phantom was allowed to reach thermal equilibrium with the degassed/deionized water to minimize conduction effects. During the high-power sonication, a continuous-wave mode of acoustic power of 44 W was applied. The duration of the sonication was 30 s. The transducer position was adjusted in order to focus at 2 cm deep inside the phantom. Post-HIFU, the phantom was dissected to look for a thermal lesion. Multiple lesions were also created in an identical phantom for repeatability purposes.

### 2.8. Temperature measurement using a thermocouple

During a high-power sonication, the temperature change at the focal point of the phantom was recorded. The temperature reader (HH806AU, Omega Engineering) was used to record the temperature change in the phantom. The thermocouple (5SC-TT-K-30–36, type K insulated beaded wire, 100  $\mu\text{m}$  thick, Omega Engineering) was inserted in the sample at the focus which was 2 cm deep. The thermocouple tip was rigid enough and it was inserted from one end of the phantom, all the way to the target with the phantom immersed in degassed/deionized water. The thermocouple tip was selected to be sufficiently thin to reduce possible artifacts. MRI artifacts were also avoided due to the size of the thermocouple. The thermocouple did not carry any electricity and therefore was considered as a passive object in the MR imaging volume. Although the focal length was known, precise localization of the focal point was achieved by changing the position of the thermocouple at low power until the highest temperature change was achieved.

### 2.9. Ultrasound and X-ray imaging

A diagnostic US imaging system (UMT-150, Shenzhen Mindray Bio-Medical Electronics Co., Ltd., Shenzhen, P.R. China) was used to image the TMM in order to check its echogenicity and homogeneity. A homogeneous piece of swine meat was US scanned with the same ultrasonic parameters to be compared with the US image of the TMM. An X-ray image was also acquired using a portable X-ray system (IMS001, Shenzhen Browiner Tech Co., Ltd., Shenzhen, P.R. China). A computed radiography (CR) reader (Vita Flex, Carestream Health, Inc., 150 Verona Street, Rochester, NY, USA) was used to digitize the latent image from the CR cassette to the computer for X-ray image reconstruction. The X-ray exposure parameters were as follows: tube current = 50 mA, tube voltage = 60 kV, and an exposure time of 320 ms.

### 2.10. MR imaging and thermometry

High-resolution MR images of the phantom were acquired after HIFU sonication in a 1.5 T MR system (Signa Excite, General Electric, Fairfield, CT, USA) using a GPFLEX coil (USA instruments, Cleveland, OH, USA). Proton density (PD) MR images were acquired with the following parameters: repetition time (TR) = 2420 ms, echo time (TE) = 41 ms, receiver bandwidth (rBW) = 15 kHz, matrix =  $256 \times 256$  pixels, slice thickness = 3 mm, number of excitations (NEX) = 7, and displayed field of view (DFOV) =  $25 \times 25$   $\text{cm}^2$ .

The temperature change in the phantom under HIFU sonication was assessed with MR thermometry. MR thermometry data was produced using single-shot EPI with the following parameters: TR = 80 ms, TE = 25.1 ms, rBW = 15 kHz, matrix =  $64 \times 64$  pixels, slice thickness = 3 mm, NEX = 1, flip angle =  $25^\circ$ , and DFOV =  $25 \times 25$   $\text{cm}^2$ .

The phantom was sonicated with the same transducer used during the thermocouple's temperature change recordings. Temperature changes were calculated using the proton resonance frequency shift method [33]. The thermometry slice was selected in a plane parallel to the propagation direction. Coronal thermal maps were initially obtained by applying low acoustical power to observe the temperature increase in the phantom and to detect the focal spot of the transducer. When the focal spot was detected, axial thermal maps were recorded to estimate the temperature change and observe the focal beam in the axial plane (parallel to the ultrasonic beam). Following analysis, a single thermal map was produced every 1.65 s. The applied acoustical power was 44 W for a sonication time of 30 s using the 2.6 MHz spherical transducer.

### 2.11. $T_1$ and $T_2$ relaxometry

The TMM was scanned in the MRI using the GPFLEX coil (USA instruments) to estimate the relaxation times. The methods to estimate the  $T_1$  and  $T_2$  relaxation times have been previously described in detail by

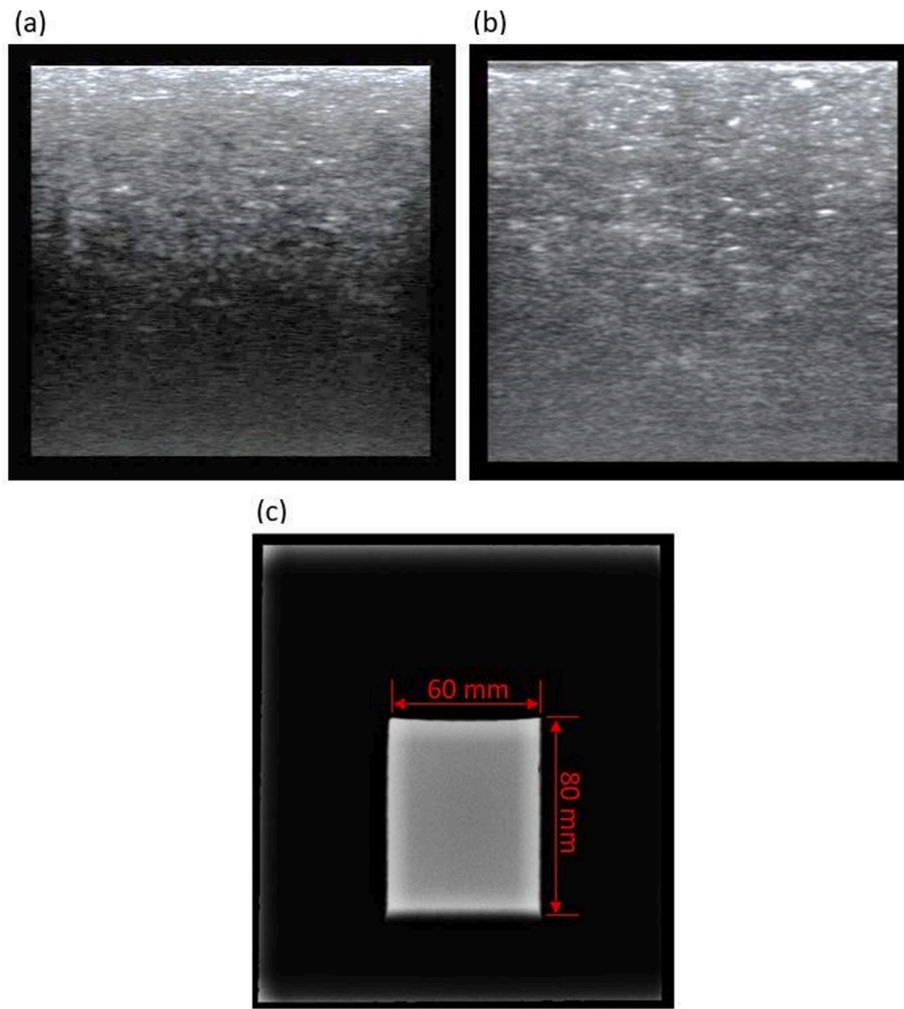


Fig. 3. (a) US image of the TMM with 2% w/v agar and 4% w/v wood powder, (b) US image of a soft tissue (swine meat), and (c) X-ray image of the TMM.

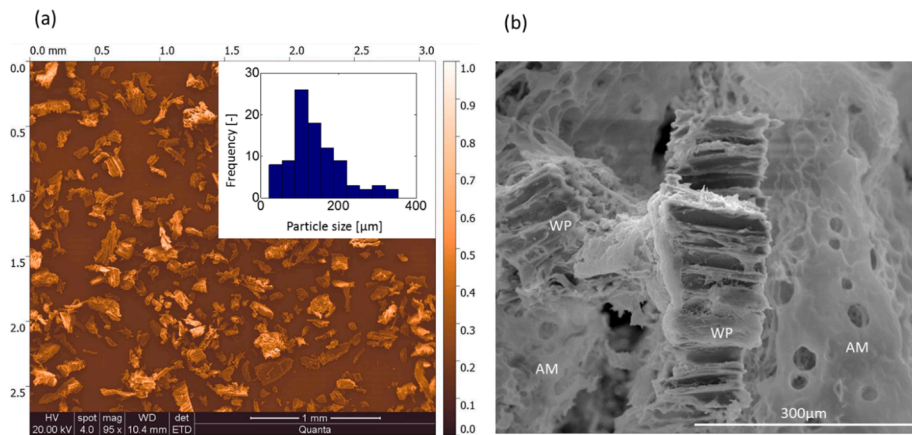


Fig. 4. SEM images of the (a) wood powder (a histogram of 92 particle length measurements is shown in inset) and, (b) agar/wood powder TMM (WP = wood powder particles, AM = agar matrix).

Menikou et al. [33]. For measuring the spin–lattice relaxation time ( $T_1$ ), an Inversion Recovery Fast Spin Echo (IR-FSE) sequence with the following acquisition parameters were used: TR = 3000 ms, TE = 45 ms, slice thickness = 5 mm, NEX = 4, matrix =  $256 \times 256$  pixels, and variable Inversion Time (TI) = 200, 400, 800, 1200, and 1600 ms.

The  $T_2$  relaxation time was estimated by obtaining a series of Fast Spin Echo (FSE) sequences for different effective echo times (23, 34, 45,

68, and 101 ms) and by calculating the inverse exponent of the exponential fit. The other MR parameters were: TR = 2500 ms, slice thickness = 5 mm, matrix =  $256 \times 256$  pixels, FOV = 16 cm, NEX = 1, and echo train length (ETL) = 4.

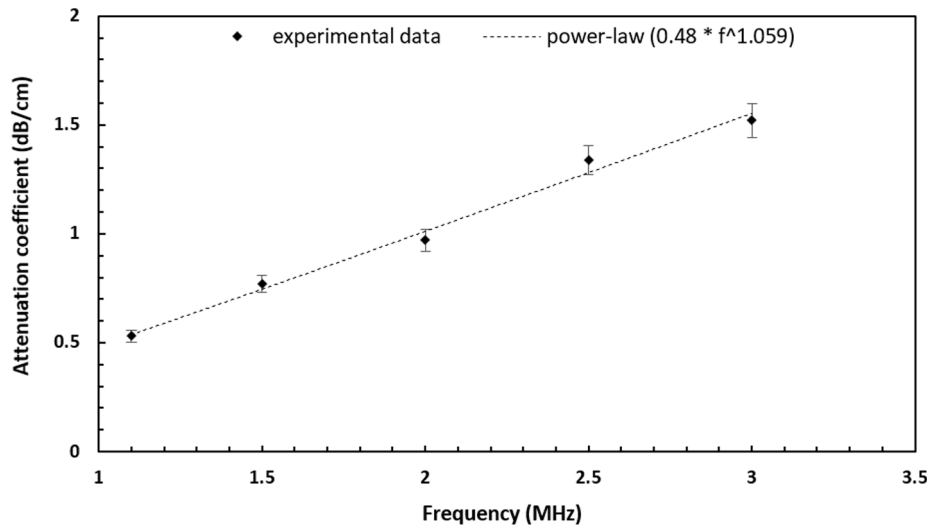


Fig. 5. Attenuation coefficient as a function of frequency for the agar/wood powder-based TMM. The mean and standard deviation are represented by the data points and the error bars respectively.

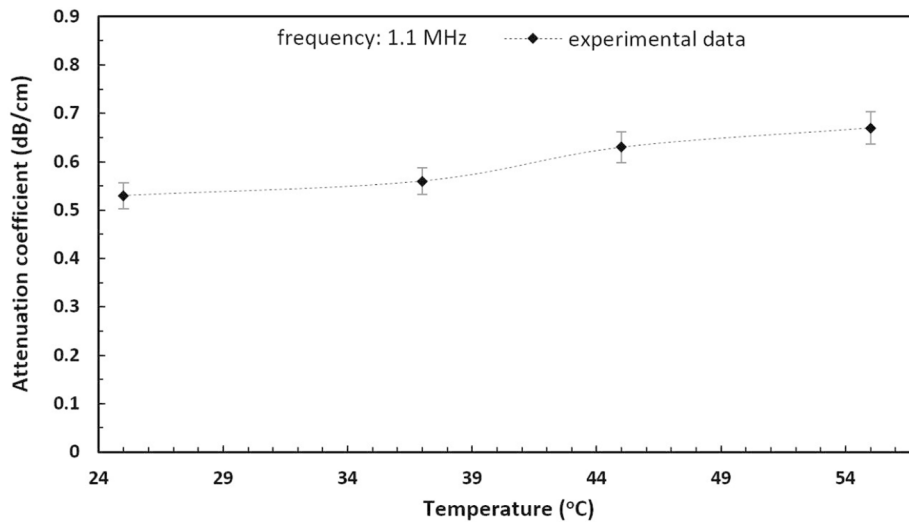


Fig. 6. Attenuation coefficient as a function of temperature for a frequency of 1.1 MHz. The mean and standard deviation are represented by the data points and the error bars respectively.

### 3. Results

An agar-based doped with wood powder TMM was prepared following a simple and fast procedure. The gel with 2% w/v agar and 4% w/v wood powder was scanned with a US imaging system (UMT-150, Shenzhen Mindray Bio-Medical Electronics Co., Ltd.) in order to demonstrate that wood powder contributes to US scattering. The scattering of the wood powder has been shown to contribute to the absorption and therefore to a total attenuation increase. The TMM appeared homogeneous with increased echogenicity as shown in Fig. 3a. Fig. 3b shows the US image of a homogeneous soft tissue (swine meat). The grey texture of the TMM resembled the sonographic appearance of normal soft tissue. Fig. 3c shows the X-ray image of the TMM.

SEM images of the wood powder and agar/wood powder TMM are illustrated in Fig. 4a and b, respectively. The wood powder particles appear elongated with aspect ratios in the range of 1–5. Statistics on the particle size were extracted by performing line measurements using the open-source software Gwyddion on the long direction of approximately 90 particles (Fig. 4a). A range of 20–350  $\mu\text{m}$  was recorded with an average particle size in the  $\sim 140$   $\mu\text{m}$  range and a standard deviation of

$\sim 70$   $\mu\text{m}$ .

A least mean square fitting was fitted on the attenuation coefficient measurements of various frequencies between 1.1 and 3 MHz. The measured attenuation coefficient ( $\alpha_0$ ) was  $0.48 \pm 0.044$  dB/cm at 1 MHz which was well within the range of equivalent values of soft tissue [34,35]. A power-law fit was determined on the data and the parameter  $n$  was found to be 1.059, which for the range of frequencies used in HIFU it is safe to assume that the attenuation coefficient of the TMM depends linearly on frequency. Fig. 5 shows the attenuation coefficient as a function of frequency. It was thought that the size of the wood powder particles ( $< 350$   $\mu\text{m}$ ) played a significant role in the value of the scattering coefficient. Wood powder particles with dimensions of the order of one wavelength of the sound wave or larger ( $\sim 0.6$  mm) are expected to diffract (beam spreading) the acoustic wave rather than scatter the wave in all directions. The attenuation coefficient for a frequency of 1.1 MHz at room temperature was found to be 0.53 dB/cm and the value remained almost unaffected at 37 °C. At higher temperatures, the attenuation coefficient slightly increased by reaching a value of 0.67 dB/cm at 55 °C. The effect of temperature on the attenuation coefficient is shown in Fig. 6.

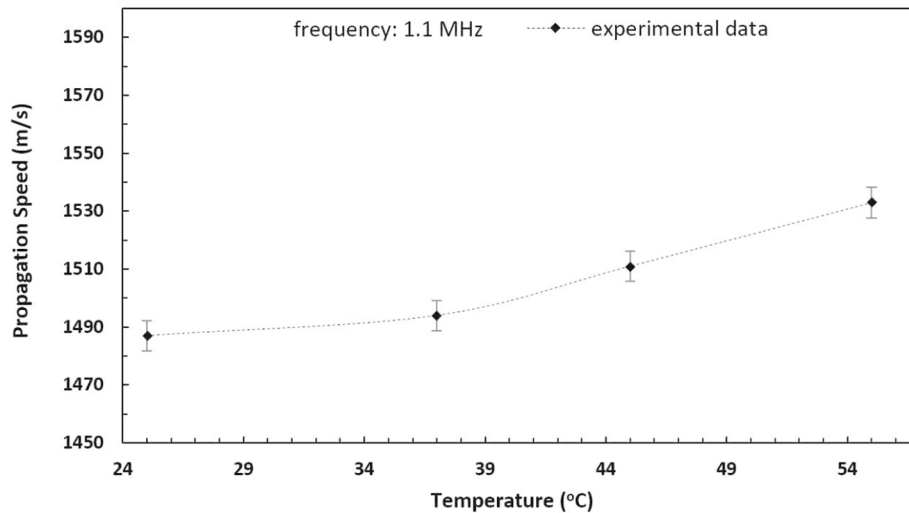


Fig. 7. Propagation speed as a function of temperature for a frequency of 1.1 MHz. The mean and standard deviation are represented by the data points and the error bars respectively.

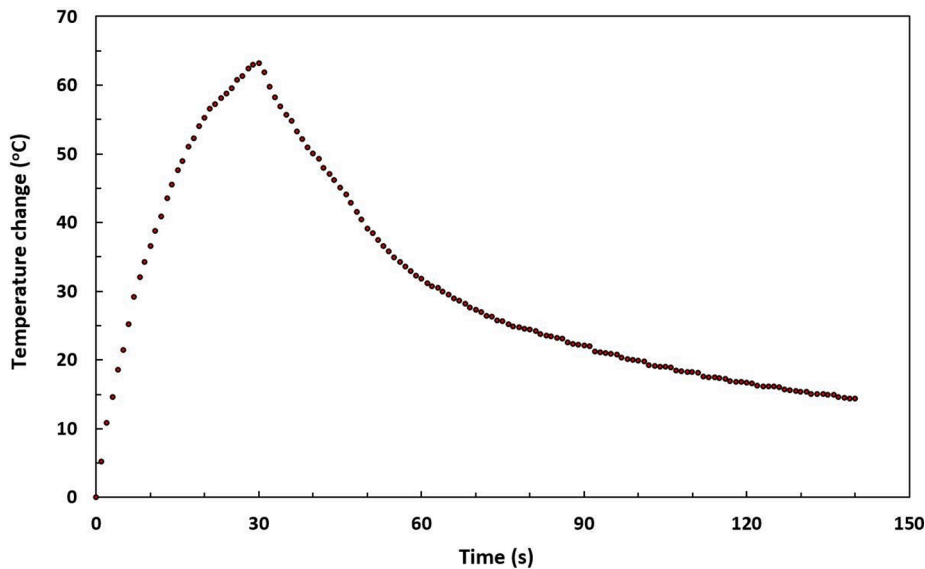


Fig. 8. Temperature change versus time that was recorded using the thermocouple by applying an acoustic power of 44 W for 30 s at a focal depth of 2 cm with the 2.6 MHz spherically-focused transducer.

Acoustic propagation speed and mass density were also assessed. The propagation speed was  $1487 \pm 5$  m/s at room temperature which is a value between the speed of sound of intra-vitum fat ( $\sim 1480$  m/s) [34] and soft tissue ( $\sim 1540$  m/s) [35]. The propagation speed increased from 1487 m/s to 1533 m/s in a temperature range between 25 and 55 °C as shown in Fig. 7. Density was calculated to be  $1060 \pm 10$  kg/m<sup>3</sup> using the water volume displacement method. Therefore, the acoustic impedance of the TMM was  $1.58 \pm 0.03$  MRayl. This result indicated an acoustic impedance close to that of muscle (1.62 MRayl) [34]. Water has an acoustic impedance of 1.54 MRayl, therefore the reflected intensity in the water/TMM interface was 0.016%.

The absorption coefficient was estimated by applying an ultrasonic protocol that produces a low-temperature change between 2 and 3 °C, which corresponded to an acoustic power of 1 W. During the sonication, the temperature increased linearly with time as expected after eliminating conduction effects. The temperature maintained its linearity (with R-squared of 0.9262) for a long sonication (30 s), which is representative of low conductivity. The maximum temperature recorded was 2.7 °C, and the rate of temperature increase was 0.045 °C/s. Based

on the temperature–time gradient, the absorption coefficient was  $0.34 \pm 0.02$  dB/cm-MHz. By subtracting the estimated absorption coefficient from the attenuation coefficient, the remaining value coefficient which is attributed to non-thermal losses is found to be 0.14 dB/cm-MHz (mostly scattering). The reflection coefficient was 0.016% based on the acoustic impedance measurement.

Thermal properties (thermal conductivity, thermal diffusivity, and specific heat capacity) were assessed by inserting a needle probe in the TMM and allow the appropriate area around the needle probe for accurate measurement. The thermal conductivity, thermal diffusivity, and specific heat capacity were estimated at  $0.51 \pm 0.005$  W/m K,  $0.29 \pm 0.0015$  mm<sup>2</sup>/s, and  $1.76 \pm 0.001$  kJ/(kg K) respectively.

Temperature change measurements were performed in the phantom using thermocouples. A temperature rise of 63 °C was achieved with a HIFU duration of 30 s and 44 W as shown in Fig. 8. After the HIFU exposure, the sonicated area showed some deterioration indicating the extent of the sonicated region. Maximum HIFU temperature changes are far less than the minimum ignition temperature of wood and therefore wood powder is considered a safe material to be used in MRgFUS



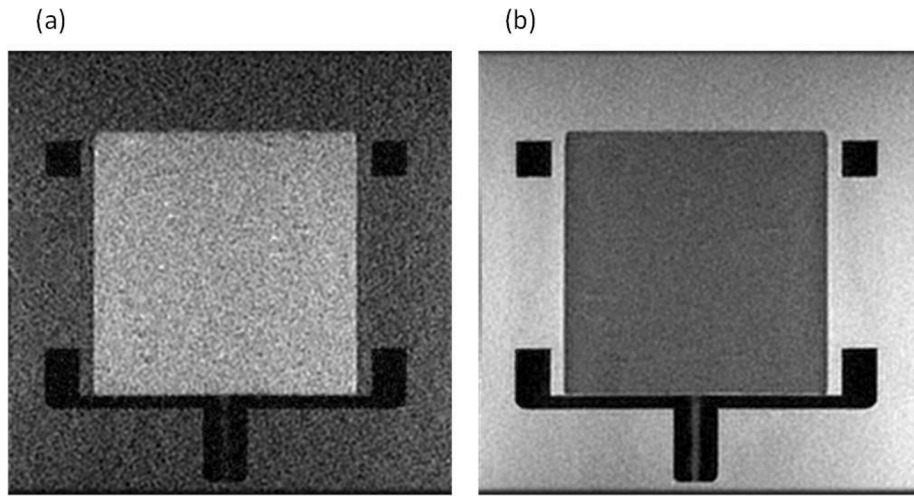


Fig. 9. (a) IR-FSE image of the TMM with TR: 3000 ms, TI: 1200 ms, and (b) T<sub>2</sub>-weighted FSE image with TR: 2500 ms, TE: 68 ms. IR-FSE and T<sub>2</sub>-weighted FSE images were acquired with various TI and TE times in order to estimate the T<sub>1</sub> and T<sub>2</sub> relaxation times respectively.

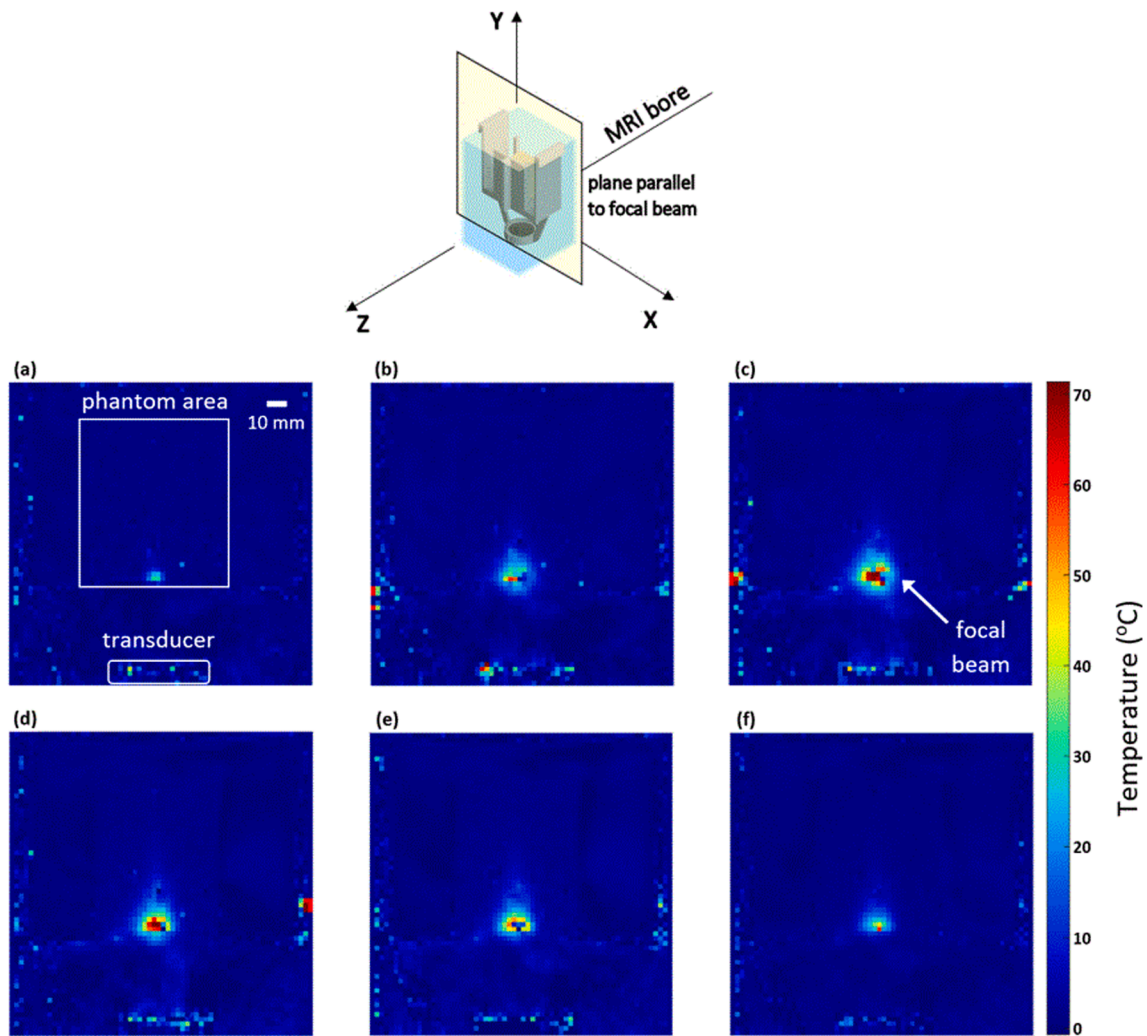


Fig. 10. MR thermal maps obtained in a plane parallel to the beam at a focal depth of 2 cm for sonication time of (a) 5 s, (b) 15 s, (c) 25 s, and (d) 30 s and for a cooling time of (e) 10 s, and (f) 18 s, respectively. The plane of the MR thermometry maps taken in relation to the direction inside the MRI is indicated.

applications.

The TMM was MR imaged using IR-T<sub>1</sub> FSE and T<sub>2</sub>-weighted FSE sequences (Fig. 9a and b) in order to estimate the T<sub>1</sub> and T<sub>2</sub> relaxation

parameters respectively. There were no severe artifacts in the vicinity of the TMM as expected. The best quality images, in terms of signal-to-noise ratio were taken and provided strong evidence that the TMM

**Table 1**

Summary of the acoustic, MR, and thermal properties of the agar/wood powder-based TMM along with the corresponding values of soft tissues and other TMMs that were found in the literature.

Property	Value	
	Agar/wood powder-based	Soft tissues/other TMMs
Attenuation coefficient	0.48 ± 0.044 dB/cm-MHz	Fat: 0.48 dB/cm-MHz [34] Liver: 0.5 dB/cm-MHz [35] Pure agar-based phantom (2% w/v): 0.18 [34] Pure PVA-based phantoms: 0.075–0.28 dB/cm-MHz [15]
Absorption coefficient	0.34 ± 0.02 dB/cm-MHz	Agar (4%)/silica (4%)/milk (30%)-based TMM: 0.22 dB/cm-MHz [32]
Propagation speed at room temperature	1487 ± 5 m/s	Soft tissues: 1478–1595 m/s [1] Intra-vitam fat: 1480 m/s [34] Pure agar-based phantom (2% w/v): 1490 m/s [19]
Mass density	1060 ± 10 kg/m <sup>3</sup>	Brain, liver, breast: 1040–1060 kg/m <sup>3</sup> [39] Muscle: 1090 kg/m <sup>3</sup> [39] Agar-based phantoms: 1030 kg/m <sup>3</sup> [19]
Acoustic impedance	1.58 ± 0.03 kg/m <sup>2</sup> s	Muscle: 1.62 MRayl [34] Agar- and polyacrylamide-based phantoms: 1.5–1.66 MRayl [41,43]
Thermal conductivity	0.51 ± 0.005 W/m K	Non-perfused muscle: 0.5–0.6 W/m.K [44]
Thermal diffusivity	0.29 ± 0.0015 mm <sup>2</sup> /s	Agar/silica phantom: 0.12–0.16 mm <sup>2</sup> /s [33,45] Acrylamide-based phantom: 0.13–0.14 mm <sup>2</sup> /s [14,41]
Specific heat capacity	1.76 ± 0.001 kJ/(kg K)	Human and animal fat: 1.6–3 kJ/(kg K) [47]
T1 relaxation time at 1.5 T	844 ms	Skeletal muscle: 868 ms, heart: 866 ms, liver: 492 ms, kidney: 652 ms [48]
T2 relaxation time at 1.5 T	66 ms	Skeletal muscle: 47 ms, heart: 57 ms, liver: 43 ms, kidney: 58 ms [48]

contained only MR compatible materials.

MR thermometry was used to calculate the maximum temperature at the focus for the same sonication protocol that was used to measure the temperature change with the thermocouple (acoustic power of 44 W for 30 s). Fig. 10 shows the estimated MR thermal maps obtained in a plane parallel to the focal beam at a depth of 2 cm. The sonication was 30 s and MR images were also acquired during the deactivation of the transducer to confirm the temperature drop. EPI sequence was used to obtain 29 MR images within a total MR scanning time of 48 s (1.65 s for each image). However, only 6 out of 29 MR images are presented in the MR thermometry results (4 during sonication and 2 during the cooling-off period). The temperature change as calculated from the thermal map at sonication of 30 s reached a value of 66.4 °C.

Following image post-processing, the nulling TI was interpolated at 585 ms and the T<sub>1</sub> was estimated at 844 ms. The T<sub>2</sub> relaxation time was found to be 66 ms. The acoustic, MR, and thermal properties of the agar-based doped with wood powder material are summarized in Table 1 along with the corresponding values of soft tissues and some TMMs. A high-resolution PD MR image was obtained after the sonication (Fig. 11a) and the sonicated area appeared brighter than the non-sonicated area. The TMM was cross-sectioned after the sonication and the sonicated brighter area was visually confirmed (Fig. 11b). The created lesion as well as its dimensions (length and diameter) are indicated in Fig. 11b. The length and diameter of the lesion were 14.5 mm and 7.8 mm respectively resulting in a ratio (length to diameter) of 1.85. Six lesions of the same HIFU parameters (44 W acoustic power for 30 s) were created as shown in Fig. 11c. The mean diameter and length of the lesions were 6.8 ± 0.5 mm and 14.4 ± 1.9 mm respectively.

A focused transducer with a lower frequency (1.1 MHz, diameter: 64 mm, focal length: 63 mm, MEDSONIC LTD) was used to produce a lesion

to a greater depth within the phantom. An acoustic power of 37.5 W was applied for 30 s sonication time at a focal depth of 2.5 cm. After the sonication, the phantom was cross-sectioned at 25 mm and a lesion of 18.8 mm length was observed as shown in Fig. 12.

#### 4. Discussion

In this study, a TMM destined to be used for MRgFUS applications has been characterized for its acoustical, MR, and thermal properties. The TMM was agar-based with the addition of a single material to control both acoustic energy loss mechanisms (absorption and scattering). This easy-to-make agar-based gel with the addition of wood powder is non-toxic, simple and quick to prepare, inexpensive cost, and possesses a high melting temperature point.

The MRI compatibility of the TMM is especially valuable since HIFU treatments are lately performed under MRI guidance [36–38]. Powdered wood with low water content produces an MRI signal with an acceptable signal-to-noise ratio. Additionally, changes in magnetic susceptibility at agar gel/wood interfaces, perturb the homogeneity of the local field and may induce artifacts capable of disturbing MR thermometry results. The issues addressed can be avoided by developing in the future a TMM of even smaller wood particles. The particle size of a sample of the wood powder was evaluated using SEM and it was estimated to be 139 ± 69 μm with a particle maximum size of 354 μm and a minimum of 22 μm.

Even though Onda Corporation produces phantoms for HIFU applications, the phantoms are expensive and a complex procedure is followed for their production. In addition, these commercial phantoms lack stability when submerged in water because they exhibit reduced rigidity. These disadvantages make them less suitable for some applications. Herein, the proposed MRgFUS TMM has good rigidity, lasts around 10 days stored in the refrigerator at a constant temperature of 4 °C, where at the end of this period it begins to dry out. However, the life of the TMM can be prolonged by the addition of preservative materials (Thimerosal or Germall-plus). The production cost of the TMM was low, therefore at the end of experimental sessions it was disposed.

The measured attenuation coefficient at 1 MHz was found to be close to fat (0.48 dB/cm-MHz) [34] and liver (0.5 dB/cm-MHz) [35]. A nearly linear frequency dependency of the attenuation coefficient has been demonstrated in a frequency range used mainly in MRgFUS applications. At body temperatures, the attenuation coefficient of the material remained almost constant relative to the same parameter at room temperature. Nevertheless, at higher temperatures, this value has shown a slightly increasing trend. The agar/wood powder TMM (manufactured with only two materials) has higher attenuation than other more complicated TMMs which have been developed and characterized over time such as agar, gelatin with the inclusion of glass bead scatterers (0.35–0.46 dB/cm-MHz) [28] and pure polyacrylamide gels (0.17–0.25 dB/cm-MHz) [34].

The measured absorption coefficient of the prescribed TMM was found to be higher by 0.12 dB/cm-MHz than an optimum recipe (4% w/v agar, 30% volume per volume evaporated milk, and 4% w/v silica) that was proposed in a previous study [32]. The goal was to increase the absorption coefficient as close as possible to 0.5 dB/cm-MHz. It was previously evidenced [32] that the absorption coefficient increases with the increase of agar concentration, evaporated milk, and silicon dioxide (until 4%). In order to observe the effect of wood powder on the absorption coefficient, a comparison between a TMM with only 2% agar and one with 2% agar and 4% wood powder was performed. The addition of 4% of wood powder increases the absorption coefficient by 0.11 dB/cm-MHz.

Measurement of the acoustic speed of the soft tissue recipe was in the lower range of biological soft tissues (1478–1595 m/s) [1] and near the value of a head-mimicking phantom that was previously proposed by our group [21]. There has been an increasing trend in the propagation speed relative to the increase in temperature. At high temperatures, the propagation speed was close to the value of soft tissue. If values closer to

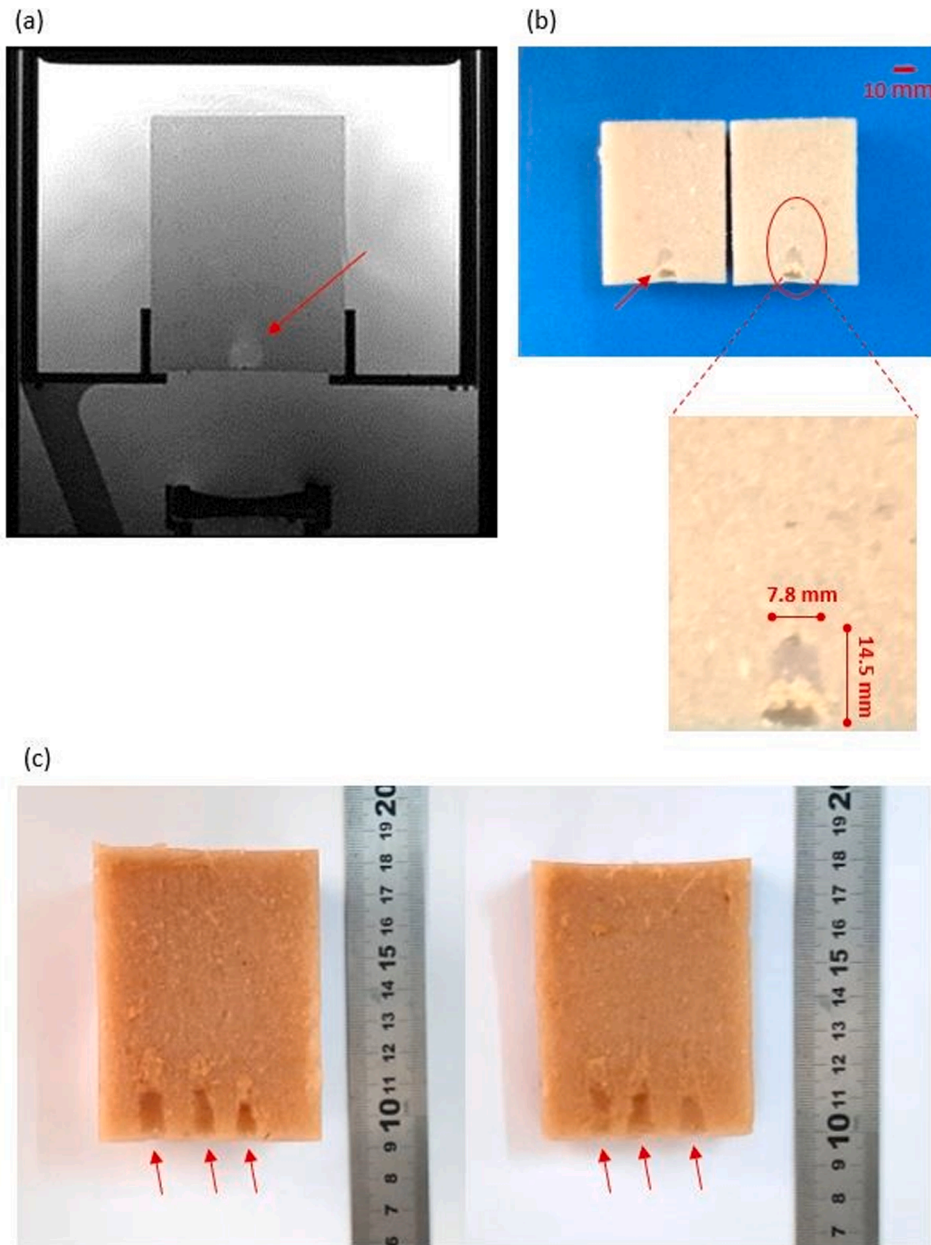


**Fig. 11.** (a) PD MR image of the TMM that was obtained after the sonication of acoustic power of 44 W for 30 s using the 2.6 MHz spherically focused transducer, and (b) Photo of the sonicated area. The TMM was vertically sliced in the middle of the focal spot. A zoomed image of the sonicated area shows the created lesion and its dimensions are indicated, and (c) Multiple lesions created in the TMM. The red arrows indicate the lesions.

1540 m/s are desired in low room temperatures, an appropriate concentration of an additive (glycerol or milk) can be added.

The mass density of the TMM ( $1060 \pm 10 \text{ kg/m}^3$ ) was found to be similar to that of the brain, liver, and breast ( $1040\text{--}1060 \text{ kg/m}^3$ ) [39] while it approximated the mass density of muscle ( $1090 \text{ Kg/m}^3$ ). Gelatin and polyacrylamide gel TMMs demonstrated mass density values within the range of soft tissues [40–42] and closed values to the proposed TMM. The acoustic impedance was in the range of other agar-based and polyacrylamide-based materials (1.5–1.66 MRayl) [41,43].

The thermal conductivity ( $0.51 \pm 0.005 \text{ W/m K}$ ) of the TMM mimics published values for non-perfused soft tissues with the value of non-perfused muscle to be in the range of 0.5–0.6 W/m K [44]. The thermal diffusivity ( $0.2935 \pm 0.0015 \text{ mm}^2/\text{s}$ ) was more than double compared to agar/silica recipe ( $0.12\text{--}0.16 \text{ mm}^2/\text{s}$ ) [33,45] and acrylamide-based ( $0.13\text{--}0.14 \text{ mm}^2/\text{s}$ ) [14,41] which are similar to the value of water ( $0.143 \text{ mm}^2/\text{s}$ ) [46]. It is concluded that wood powder

also contributes to the increase of the TMM's thermal diffusivity. The high thermal diffusivity shows how quickly the material transfers heat across HIFU temperatures. Specific heat capacity was in the range of the values of human and animal fat [47].

From the US images, it was shown that the addition of wood powder increased the echogenicity of the TMM, such that it closely resembled the US signal generated by real tissues. Additionally, the TMM fulfilled the requirement of being compatible with an MRI scanner. The measured relaxation times  $T_1$  and  $T_2$  were within the range of values found in the literature for soft tissue [48].

MRI and optical images of the TMM indicate that HIFU ablation at high power levels can lead to the formation of focal lesion. The formation of focal lesion in MRI images appears to be hyperintense. The TMM allows the lesions to be optically observed and measured. However, high power sonications cause irreversible damage to the phantom, whilst in low power settings the absence of any material deterioration



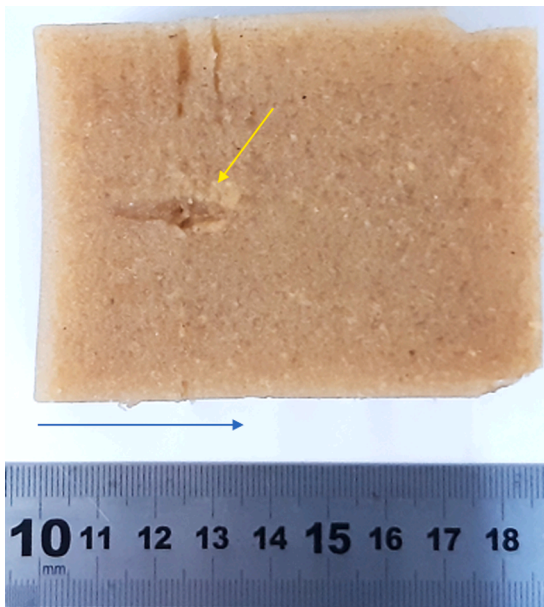


**Fig. 12.** A lesion was formed on a plane parallel to the ultrasound beam after HIFU exposure at acoustic power of 37.5 W for a sonication time of 30 s using a 1.1 MHz focused transducer at 2.5 cm focal depth. The yellow arrow indicates the lesion and the blue arrow indicates the beam direction.

demonstrated its suitability of being used repeatedly. Additionally, the possibility of inserting thermocouples to measure temperature rise and check transducers' performance without affecting its structural integrity was another feature of the phantom. The temperature rise measured with the thermocouple was confirmed with MR thermometry. Both thermocouple and MR thermometry yielded almost identical temperature change readings for a specific ultrasonic protocol (63 and 66.4 °C respectively). There is always a possibility that the acoustic field is distorted by the metal-base thermocouple wire, which can induce a focus shift observed as a peak temperature decrease. Positioning of the thermocouple is done manually and although all possible measures are followed to target the nominal focal region, the procedure is always prone to mispositioning errors. The main advantage of using this method is the relatively low noise of the temperature-time profile compared to MR thermometry. On the other hand, the reliability of MR thermometry results is related to the signal-to-noise ratio of the phase images which is usually limiting since the imaging coils are not optimized for the phantom's geometry. External interferences that induce inhomogeneities to the MR static field are also sources of error in MR thermometry. Mispositioning of single slice MR thermometry especially in the long axis and partial volume effect are also factors that can underestimate peak temperature.

Finally, the length to diameter ratio showed that a good-shaped lesion was created and cavitation was not affecting. The expected focal beam was at a depth of 20 mm. However, the focal beam shifted 10 mm to the front surface of the TMM. Higher penetration of the US beam can be achieved using a transducer with a lower frequency (0.5–1 MHz). This was achieved by using a transducer with lower frequency and lesion was created to a greater depth in the phantom. Multiple lesions were produced indicating repeatability of the lesions' dimensions.

## 5. Conclusions

A complete characterization of an agar-based TMM doped with wood powder destined for evaluation of MRgFUS protocols was presented. The characterization included measurements of the acoustical, MR, and thermal properties of the TMM. The goal of this work was to develop an agar-based TMM doped with a single material in order to achieve a

higher absorption coefficient than other agar-based TMMs doped with various additives. However, the effect of the particle size of the wood powder on the acoustical, MR, and thermal properties of the TMM should be investigated further in upcoming studies. Finally, the TMM has the ability to model the formation of thermal lesions above the temperature threshold which is still unknown. In the future, when the threshold is determined it will be possible to estimate the ultrasonic energy that is needed to produce a lesion in the TMM. Future studies will entail adding materials to change the agar/wood powder TMM properties to match the properties of specific tissues of interest.

## Ethical approval

This article does not contain any studies with human participants or animals performed by any of the authors.

## Declaration of Competing Interest

The authors declare that they have no known competing financial interests or personal relationships that could have appeared to influence the work reported in this paper.

## Acknowledgements

The study has been funded under the Restart 2016-2020 program, with the support of the Cyprus Research and Innovation foundation, and the European Structural Funds under the project SOUNDPET (INTEGRATED/0918/0008).

## References

- [1] M.O. Culjat, D. Goldenberg, P. Tewari, R.S. Singh, A review of tissue substitutes for ultrasound imaging, *Ultrasound Med. Biol.* 36 (6) (2010) 861–873, <https://doi.org/10.1016/j.ultrasmedbio.2010.02.012>.
- [2] L. Hofstetter, L. Fausett, A. Mueller, H. Odeen, A.H. Payne, D.A. Christensen, D. L. Parker, Development and characterization of a tissue mimicking psyllium husk gelatin phantom for ultrasound and magnetic resonance imaging, *Int. J. Hyperthermia* 37 (1) (2020) 283–290, <https://doi.org/10.1080/02656736.2020.1739345>.
- [3] T.J. Hall, M. Bilgen, M.F. Insana, T.A. Krouskop, Phantom materials for elastography, *IEEE Trans. Ultrason., Ferroelectr., Freq. Control* 44 (6) (1997) 1355–1365, <https://doi.org/10.1109/58.656639>.
- [4] A. Dabbagh, B.J.J. Abdullah, C. Ramasindarum, N.H.A. Kasim, Tissue-mimicking gel phantoms for thermal therapy studies, *Ultrason. Imaging* 36 (4) (2014) 291–316, <https://doi.org/10.1177/0161734614526372>.
- [5] J.R. Cook, R.R. Bouchard, S.Y. Emelianov, Tissue-mimicking phantoms for photoacoustic and ultrasound imaging, *Biomed. Opt. Express* 2 (11) (2011) 3193–3206, <https://doi.org/10.1364/BOE.2.003193>.
- [6] E.L. Madsen, J.A. Zagzebski, R.A. Banjavie, R.E. Jutila, Tissue mimicking materials for ultrasound phantoms, *Med Phys.* 5 (5) (1978) 391–394, <https://doi.org/10.1118/1.594483>.
- [7] K. Takegami, Y. Kaneko, T. Watanabe, T. Maruyama, Y. Matsumoto, H. Nagawa, Polyacrylamide gel containing egg white as new model for irradiation experiments using focused ultrasound, *Ultrasound Med. Biol.* 30 (10) (2004) 1419–1422, <https://doi.org/10.1016/j.ultrasmedbio.2004.07.016>.
- [8] J.M. Choi, S.R. Guntur, K.I. Lee, D.G. Paeng, A. Coleman, A tissue mimicking polyacrylamide hydrogel phantom for visualizing thermal lesions generated by high intensity focused ultrasound, *Ultrasound Med. Biol.* 39 (3) (2013) 439–448, <https://doi.org/10.1016/j.ultrasmedbio.2012.10.002>.
- [9] C. Lafon, V. Zderic, M.L. Noble, et al., Gel phantom for use in high-intensity focused ultrasound dosimetry, *Ultrasound Med. Biol.* 31 (10) (2005) 1383–1389, <https://doi.org/10.1016/j.ultrasmedbio.2005.06.004>.
- [10] M. McDonald, S. Lochhead, R. Chopra, M. Bronskill, Multi-modality tissue-mimicking phantom for thermal therapy, *Phys. Med. Biol.* 49 (13) (2004) 2767–2778, <https://doi.org/10.1088/0031-9155/49/13/001>.
- [11] M. Bini, A. Ignesti, L. Millanta, R. Olmi, N. Rubino, R. Vanni, The polyacrylamide as a phantom material for electromagnetic hyperthermia studies, *IEEE Trans. Biomed. Eng.* 31 (3) (1984) 317–322, <https://doi.org/10.1109/TBME.1984.325271>.
- [12] ONDA Corporation, HIFU Phantom Gel, [http://www.ondacorp.com/images/brochures/Onda\\_GelPhantom\\_DataSheet.pdf](http://www.ondacorp.com/images/brochures/Onda_GelPhantom_DataSheet.pdf) 2012 (accessed 20 March 2020).
- [13] M.K. Sun, J. Shieh, C.W. Lo, et al., Reusable tissue-mimicking hydrogel phantoms for focused ultrasound ablation, *Ultrason. Sonochem.* 23 (2015) 399–405, <https://doi.org/10.1016/j.ulsonch.2014.10.008>.
- [14] A. Eranki, A.S. Mikhail, A.H. Negussie, P.S. Katti, B.J. Wood, A. Partanen, Tissue-mimicking thermo-chronic phantom for characterization of HIFU devices and



- applications, *Int. J. Hyperthermia* 36 (1) (2019) 517–528, <https://doi.org/10.1080/02656736.2019.1605458>.
- [15] K.J.M. Surry, H.J.B. Austin, A. Fenster, T.M. Peters, Poly(vinyl alcohol) cryogel phantoms for use in ultrasound and MRI imaging, *Phys. Med. Biol.* 49 (24) (2004) 5529–5546, <https://doi.org/10.1088/0031-9155/49/24/009>.
- [16] W. Xia, D. Piras, M. Heijblom, W. Steenbergen, T.G. van Leeuwen, S. Manohar, Poly(vinyl alcohol) gels as photoacoustic breast phantoms revisited, *J. Biomed. Opt.* 16 (7) (2011), 075002, <https://doi.org/10.1117/1.3597616>.
- [17] G. Wojcik, T. Szabo, J. Mould, L. Carcione, F. Clougherty, Nonlinear pulse calculations and data in water and a tissue mimic, in: *Proceedings of the IEEE Ultrasonics Symposium 2, 1999*, pp. 1521–1526, <https://doi.org/10.1109/ULTSYM.1999.849286>.
- [18] M. Earle, G. De Portu, E. De Vos, Agar ultrasound phantoms for low-cost training without refrigeration, *Afr. J. Emerg. Med.* 6 (1) (2016) 18–23, <https://doi.org/10.1016/j.afjem.2015.09.003>.
- [19] E.L. Madsen, G.R. Frank, F. Dong, Liquid or solid ultrasonically tissue-mimicking materials with very low scatter, *Ultrasound Med. Biol.* 24 (4) (1998) 535–542, [https://doi.org/10.1016/s0301-5629\(98\)00013-1](https://doi.org/10.1016/s0301-5629(98)00013-1).
- [20] G. Menikou, M. Yiannakou, C. Yiallouras, C. Ioannides, C. Damianou, MRI-compatible breast/rib phantom for evaluating ultrasonic thermal exposures, *Int. J. Med. Robot* 14 (1) (2017), <https://doi.org/10.1002/rcs.1849>.
- [21] G. Menikou, T. Dadakova, M. Pavlina, M. Bock, C. Damianou, MRI compatible head phantom for ultrasound surgery, *Ultrasonics* 57 (2015) 144–152, <https://doi.org/10.1016/j.ultras.2014.11.004>.
- [22] R. Concalves, A.J. Trinca, G.C. dos Santos Ferreira, Effect of coupling media on velocity and attenuation of ultrasonic waves in Brazilian wood, *J. Wood Sci.* 57 (2011) 282–287, <https://doi.org/10.1007/s10086-011-1177-y>.
- [23] H. Berndt, G.C. Johnson, Examination of wave propagation in wood from a microstructural perspective, *Rev. Progr. Quant. Nondestruct. Eval.* 14 (1995) 1661–1668, [https://doi.org/10.1007/978-1-4615-1987-4\\_213](https://doi.org/10.1007/978-1-4615-1987-4_213).
- [24] F. Liu, P. Xu, H. Zhang, C. Guan, D. Feng, X. Wang, Use of time-of-flight ultrasound to measure wave speed in poplar seedlings, *Forests* 10 (8) (2019) 17, <https://doi.org/10.3390/f10080682>.
- [25] H. Sakai, K. Takagi, A. Minanisawa, Ultrasonic properties in woods, *Jpn. J. Appl. Phys.* 27 (1988) 55–57.
- [26] E.Y. Sari, P. Nasution, F. Ramdhan, Characteristics of physical properties of wood powder composites and bagasseas construction materials of ship, *SPERMONDE 5* (1) (2019) 11–15, <https://doi.org/10.20956/jjks.v5i1.7038>.
- [27] B. Ababneh, A.A. Tajuddin, R. Hashim, I.L. Shuaib, S.M. Isa, A. AL-Jarrah, Evaluation of the relaxation times for Rhizophora spp. Wood as human tissue equivalent for MRI breast phantom, *Asian J. Appl. Sci.* 3(6) (2015) 759–764.
- [28] E.L. Madsen, M.A. Hobson, H. Shi, T. Varghese, G.R. Frank, Tissue-mimicking agar/gelatin materials for use in heterogeneous elastography phantoms, *Phys. Med. Biol.* 50 (23) (2005) 5597–5618, <https://doi.org/10.1088/0031-9155/50/23/013>.
- [29] D. Nečas, P. Klapek, Gwyddion: an open-source software for SPM data analysis, *Cent. Eur. J. Phys.* 10 (1) (2012) 181–188.
- [30] E.L. Madsen, J.A. Zagzebski, G.R. Frank, Oil-in-gelatin dispersions for use as ultrasonically tissue-mimicking materials, *Ultrasound Med. Biol.* 8 (3) (1982) 277–287, [https://doi.org/10.1016/0301-5629\(82\)90034-5](https://doi.org/10.1016/0301-5629(82)90034-5).
- [31] A. Keshavarzi, S. Vaezy, P.J. Kaczkowski, et al., Attenuation coefficient and sound speed in human myometrium and uterine fibroid tumors, *J. Med. Ultrasound* 20 (5) (2001) 473–480, <https://doi.org/10.7863/jum.2001.20.5.473>.
- [32] T. Drakos, M. Giannakou, G. Menikou, C. Ioannides, C. Damianou, An improved method to estimate ultrasonic absorption in agar-based gel phantom using thermocouples and MR thermometry, *Ultrasonics* 103 (2020), 106089, <https://doi.org/10.1016/j.ultras.2020.106089>.
- [33] G. Menikou, C. Damianou, Acoustic and thermal characterization of agar based phantoms used for evaluating focused ultrasound exposures, *J. Ther. Ultrasound* 5 (2017) 14, <https://doi.org/10.1186/s40349-017-0093-z>.
- [34] A. Cafarelli, A. Verbeni, A. Poliziani, P. Dario, A. Menciaci, L. Ricotti, Tuning acoustic and mechanical properties of materials for ultrasound phantoms and smart substrates for cell cultures, *Acta Biomater.* 49 (2016) 368–378, <https://doi.org/10.1016/j.actbio.2016.11.049>.
- [35] S. Mueller, L. Sandrin, Liver stiffness: a novel parameter for the diagnosis of liver disease, *Hepat. Med.* 2 (2010) 49–67, <https://doi.org/10.2147/hmer.s7394>.
- [36] A.E. Stewart, J. Rabinovici, M.C. Tempany, Y. Inbar, L. Regan, B. Gostout, Clinical outcomes of focused ultrasound surgery for the treatment of uterine fibroids, *Fertil. Steril.* 85 (1) (2006) 22–29, <https://doi.org/10.1016/j.fertnstert.2005.04.072>.
- [37] A. Blana, B. Walter, S. Rogenhofer, F.W. Wieland, High-intensity focused ultrasound for the treatment of localized prostate cancer, *Urology* 63 (2) (2004) 297–300, <https://doi.org/10.1016/j.urology.2003.09.020>.
- [38] J.W. Elias, D. Huss, T. Voss, J. Loomba, M. Khaled, E. Zadicario, A pilot study of focused ultrasound thalamotomy for essential tremor, *N. Engl. J. Med.* 369 (7) (2013) 640–648, <https://doi.org/10.1056/NEJMoa1300962>.
- [39] A. P. Haggall, F. Gennaro, C. Baumgartner, E. Neufeld, C.M. Gosselin, D. Payne, IT<sup>2</sup>S Database for thermal and electromagnetic parameters of biological tissues, Version 2.6, [www.itis.ethz.ch/database](http://www.itis.ethz.ch/database), 2015 (accessed 26 March 2020).
- [40] Z. Bu-Lin, H. Bing, K. Sheng-Li, Y. Huang, W. Rong, L. Jia, A polyacrylamide gel phantom for radiofrequency ablation, *Int. J. Hyperthermia* 24 (7) (2008) 568–576, <https://doi.org/10.1080/02656730802104732>.
- [41] C. Lafon, J.P. Kaczkowski, S. Vaezy, M. Noble, A.O. Sapozhnikov, Development and characterization of an innovative synthetic tissue-mimicking material for high intensity focused ultrasound (HIFU) exposures, in: *IEEE Ultrasonics Symposium, Atlanta, 2001*, <https://doi.org/10.1109/ULTSYM.2001.991957>.
- [42] P.M. Robinson, J.M. Richardson, L.J. Green, W.A. Preece, New materials for dielectric simulation of tissues, *Phys. Med. Biol.* 36 (12) (1991) 1565–1571, <https://doi.org/10.1088/0031-9155/36/12/002>.
- [43] P.C. Labuda, C.C. Church, Augmentation of HIFU-induced heating with fibers embedded in a phantom, *Ultrasound Med. Biol.* 37 (3) (2011) 442–449, <https://doi.org/10.1016/j.ultrasmedbio.2010.12.010>.
- [44] J. Crezee, J.J. Legendijk, Temperature uniformity during hyperthermia: the impact of large vessels, *Phys. Med. Biol.* 37 (6) (1992) 1321–1337, <https://doi.org/10.1088/0031-9155/37/6/009>.
- [45] Y.C. Lai, E.D. Kruse, F.C. Caskey, N.D. Stephens, L.P. Sutcliffe, W.K. Ferrara, Noninvasive thermometry assisted by a dual-channel ultrasound transducer for mild hyperthermia, *IEEE Trans. Ultrason., Ferroelectr., Freq. Control* 57 (12) (2010) 2671–2684, <https://doi.org/10.1109/TUFFC.2010.1741>.
- [46] J. Blumm, A. Lindemann, Characterization of the thermophysical properties of molten polymers and liquids using the flash technique, *High Temp. High Press.* 35 (6) (2003) 627–632, <https://doi.org/10.1118/1.595535>.
- [47] K. Giering, I. Lamprecht, O. Minet, Specific heat capacities of human and animal tissues, in: *Proc. SPIE 2624, Laser-Tissue Interaction and Tissue Optics, 1996*, <https://doi.org/10.1117/12.229547>.
- [48] A.P. Bottomley, H.T. Foster, E.R. Argersinger, M.L. Pfeiffer, A review of normal tissue hydrogen NMR relaxation times and relaxation mechanisms from 1–100 MHz: dependence on tissue type, NMR frequency, temperature, species, excision and age, *Med. Phys.* 11 (4) (1984) 425–448, <https://doi.org/10.1118/1.595535>.